

INFRARED RENORMALONS AND SINGLE MESON PRODUCTION IN PROTON-PROTON COLLISIONS

A. I. Ahmadov^{1 *}, Coskun Aydin^{3 †}, Sh. M.

Nagiyev², Yilmaz A. Hakan^{3 ‡}, and E. A. Dadashov²

¹ *Department of Theoretical Physics, Baku State University,*

Z. Khalilov st. 23, AZ-1148, Baku, Azerbaijan

²*Institute of Physics of Azerbaijan National Academy of Sciences, Baku, Azerbaijan*

³ *Department of Physics, Karadeniz Technical University, Trabzon, Turkey*

Abstract

In this article, we investigate the contribution of the higher twist Feynman diagrams to the large- p_T inclusive pion production cross section in proton-proton collisions and present the general formulae for the higher twist differential cross sections in the case of the running coupling and frozen coupling approaches. The structure of infrared renormalon singularities of the higher twist subprocess cross section and the resummed expression (the Borel sum) for it are found. We compared the resummed higher twist cross sections with the ones obtained in the framework of the frozen coupling approximation and leading twist cross section. We obtain, that ratio R for all values of the transverse momentum p_T of the pion identical equivalent to ratio r . It is shown that the resummed result depends on the choice of the meson wave functions used in calculation. Phenomenological effects of the obtained results are discussed.

PACS numbers: 12.38.-t, 13.60.Le, 14.40.Aq, 13.87.Fh,

Keywords: higher twist, infrared renormalons, pion wave function

* E-mail: ahmadovazar@yahoo.com

† E-mail: coskun@ktu.edu.tr

‡ E-mail: hakany@ktu.edu.tr

I. INTRODUCTION

The large-order behavior of a perturbative expansion in gauge theories is inevitably dominated by the factorial growth of renormalon diagrams [1-4]. In the case of quantum chromodynamics (QCD), the coefficients of perturbative expansions in the QCD coupling α_s can increase dramatically even at low orders. This fact, together with the apparent freedom in the choice of renormalization scheme and renormalization scales, limits the predictive power of perturbative calculations, even in applications involving large momentum transfer, where α_s is effectively small.

A number of theoretical approaches have been developed to reorganize the perturbative expansions in a effort to improve the predictability of the perturbative QCD(pQCD). For example, optimized scale and scheme choices have been proposed, such as the method of effective charges (ECH) [5], the principle of minimal sensitivity (PMS) [6], and the Brodsky-Lepage- Mackenzie (BLM) scale-setting prescription [7] and its generalizations [8-20]. In [4] developments include the resummation of the formally divergent renormalon series and the parametrization of related higher twist power-suppressed contributions.

In general, a factorially divergent renormalon series arises when one integrates over the logarithmically running coupling $\alpha_s(k^2)$ in a loop diagram. Such contributions do not occur in conformally invariant theories which have a constant coupling. Of course, in the physical theory, the QCD coupling does run.

One of the fundamental achievements of QCD is the prediction of asymptotic scaling laws for large-angle exclusive processes and their calculation in the framework of perturbative QCD [21-23]. In the context of the factorized QCD an expression for an amplitude of an exclusive process can be written as integral over x, y of hadron wave functions $\Phi_i(x, \hat{Q}^2)$ (an initial hadron) and $\Phi_f^*(y, \hat{Q}^2)$ (a final hadron) and amplitude $T_H(x, y; \alpha_s(\hat{Q}^2), Q^2)$ of the hard-scattering subprocess [22]. The hard-scattering amplitude $T_H(x, y; \alpha_s(\hat{Q}^2), Q^2)$ depends on a process and can be obtained in the framework of pQCD, whereas the wave function $\Phi(x, \hat{Q}^2)$ describes all the non-perturbative and process-independent effects of hadronic binding. The hadron wave function gives the amplitude for finding partons (quarks, gluons) carrying the longitudinal fractional momenta $\mathbf{x} = (x_1, x_2, \dots, x_n)$ and virtualness up to \hat{Q}^2 within the hadron and, in general, includes all Fock state ($q_1\bar{q}_2$ -for mesons, uud -for proton, etc.) contributions to the leading scaling behavior, other Fock states' contributions are suppressed

by powers of $1/Q^2$. In our work we shall restrict ourselves by considering the lowest Fock state for a meson. Then, $x = x_1, x_2$ and $x_1 + x_2 = 1$.

This approach can be applied for investigation, not only exclusive processes but also for the calculation of higher twist (HT) corrections to some inclusive processes, such as large - p_T dilepton production [24], two-jet+meson production in the electron-positron annihilation [25], etc. In these early papers for calculation of integrals over $x = x_1, x_2$, like

$$I \sim \int \alpha_s(\hat{Q}^2) \Phi(x, \hat{Q}^2) F(x, \alpha_s(\hat{Q}^2), Q^2) \delta(1 - x_1 - x_2) dx_1 dx_2 \quad (1.1)$$

which appear in an expression of the amplitude, the frozen coupling constant approximation was used. Some comments are in order concerning this point. It is well known [7], that in pQCD calculations the argument of the QCD coupling constant (or the renormalization and factorization scale) \hat{Q}^2 should be taken equal to the square of the momentum transfer of a hard gluon in a corresponding Feynman diagram. But defined in this way, $\alpha_s(\hat{Q}^2)$ suffers from infrared singularities. For example in our work [26], \hat{Q}^2 equals to $(x_1 - 1)\hat{u}$ and $-x_1\hat{t}$, where \hat{u} , \hat{t} are the subprocess's Mandelstam invariants. Therefore, in the soft regions $x_1 \rightarrow 0$, $x_2 \rightarrow 0$ integrals (1.1) diverge and for their calculation some regularization methods of $\alpha_s(Q^2)$ in these regions are needed. The power-suppressed corrections arising from the soft end-point regions to the single meson photoproduction process were computed in [27]. In Ref. [27] the evolution of the meson DAs on factorization scale was ignored. In the present work take into account this evolution as well. Investigation of the infrared renormalon effects in various inclusive and exclusive processes is one of the important and interesting problems in the perturbative QCD. It is known that infrared renormalons are responsible for factorial growth of coefficients in perturbative series for the physical quantities. But, these divergent series can be resummed by means of the Borel transformation [1] and the principal value prescription [28] and effects of infrared renormalons can be taken into account by scale-setting procedure $\alpha_s(Q^2) \rightarrow \alpha_s(\exp(f(Q^2))Q^2)$ at the one-loop order results. Technically, all-order resummation of infrared renormalons corresponds to the calculation of the one-loop Feynman diagrams with the running coupling constant $\alpha_s(-k^2)$ at the vertices or, alternatively, to calculation of the same diagrams with non-zero gluon mass. Studies of infrared renormalon problems have opened also new prospects for evaluation of power suppressed corrections to processes characteristics [29].

By taking these points into account, it may be asserted that the analysis of the higher

twist effects on the dependence of the pion wave function in pion production at proton-proton collisions by the running coupling (RC) method, where these singularities had been regularized by means of the principal value prescription [28] are significant in both theoretical and experimental studies.

Another important aspect of this study is the choice of the meson model wave functions. In this respect, the contribution of the higher twist Feynman diagrams to a pion production cross section in proton-proton collisions has been computed by using various pion wave functions. Also, higher twist contributions which calculated by the running coupling constant and frozen coupling constant methods have been estimated and compared to each other. Within this context, this paper is organized as follows: in section II, we provide some formulae for the calculation of the contribution of the high twist diagrams. In section III we present some formulae and analysis of the higher twist effects on the dependence of the pion wave function by the running coupling constant method, in section IV, we provide some formulae for the calculation of the contribution of the leading twist diagrams and in section V, we present the numerical results for the cross section and discuss the dependence of the cross section on the pion wave functions. We state our conclusions in section VI.

II. CONTRIBUTION OF THE HIGH TWIST DIAGRAMS

The higher twist Feynman diagrams, which describe the subprocess $q_1 + \bar{q}_2 \rightarrow \pi^+(\pi^-) + \gamma$ for the pion production in the proton-proton collision are shown in Fig.1. In the higher twist diagrams, the pion of a proton quark is directly observed. Their $1/Q^2$ power suppression is caused by a hard gluon exchange between pion constituents. The amplitude for this subprocess can be found by means of the Brodsky-Lepage formula [22]

$$M(\hat{s}, \hat{t}) = \int_0^1 dx_1 \int_0^1 dx_2 \delta(1 - x_1 - x_2) \Phi_\pi(x_1, x_2, Q^2) T_H(\hat{s}, \hat{t}; x_1, x_2). \quad (2.1)$$

In Eq.(2.1), T_H is the sum of the graphs contributing to the hard-scattering part of the subprocess. The hard-scattering part for the subprocess under consideration is $q_1 + \bar{q}_2 \rightarrow (q_1 \bar{q}_2) + \gamma$, where a quark and antiquark form a pseudoscalar, color-singlet state ($q_1 \bar{q}_2$). The hard-scattering amplitude $T_H(\hat{s}, \hat{t}; x_1, x_2)$ depends on a process and can be obtained in the framework of pQCD, whereas the wave function $\Phi_\pi(x_1, x_2, Q^2)$ describes all the non-perturbative and process-independent effects of hadronic binding. The hadron wave function

gives the amplitude for finding partons (quarks, gluons) carrying the longitudinal fractional momenta $\mathbf{x} = (x_1, x_2, \dots, x_n)$ and virtualness up to Q^2 within the hadron and, in general, includes all Fock states with quantum numbers of the hadron. But only the lowest Fock state ($q_1\bar{q}_2$ -for mesons, uud -for proton, *etc.*) contributes to the leading scaling behavior, other Fock state contributions are suppressed by powers of $1/Q^2$. In our work, we have restricted ourselves to considering the lowest Fock state for a meson. Then $\mathbf{x} = x_1, x_2$ and $x_1 + x_2 = 1$. This approach can be applied not only to the investigation of exclusive processes, but also to the calculation of higher twist corrections to some inclusive processes. The $q_1\bar{q}_2$ spin state used in computing T_H may be written in the form

$$\sum_{s_1, s_2} \frac{u_{s_1}(x_1 p_M) \bar{v}_{s_2}(x_2 p_M)}{\sqrt{x_1} \sqrt{x_2}} \cdot N_{s_1 s_2}^s = \begin{cases} \frac{\gamma_5 \hat{p}_\pi}{\sqrt{2}}, \pi, \\ \frac{\hat{p}_M}{\sqrt{2}}, \rho_L \text{ helicity } 0, \\ \mp \frac{\varepsilon_\pm \hat{p}_M}{\sqrt{2}}, \rho_T \text{ helicity } \pm 1, \end{cases} \quad (2.2)$$

where $\varepsilon_\pm = \mp(1/\sqrt{2})(0, 1, \pm i, 0)$ in a frame with $(p_M)_{1,2} = 0$ and the $N_{s_1 s_2}^s$ project out a state of a spin s , and p_M is the four-momentum of the final meson. In our calculation, we have neglected the pion and the proton masses. Turning to extracting the contributions of the higher twist subprocesses, there are many kinds of leading twist subprocesses in pp collisions as the background of the higher twist subprocess $q_1 + q_2 \rightarrow \pi^+ (\text{or } \pi^-) + \gamma$, such as $q + \bar{q} \rightarrow \gamma + g (g \rightarrow \pi^+ (\pi^-))$, $q + g \rightarrow \gamma + q (q \rightarrow \pi^+ (\pi^-))$, $\bar{q} + g \rightarrow \gamma + \bar{q} g (\bar{q} \rightarrow \pi^+ (\pi^-))$ and *ets.* The contributions from these leading twist subprocesses strongly depend on some phenomenological factors, for example, quark and gluon distribution functions in the proton and fragmentation functions of various constituents *etc.* Most of these factors have not been well determined, neither theoretically nor experimentally. Thus they cause very large uncertainty in the computation of the cross section of process $pp \rightarrow \pi^+ (\text{or } \pi^-) + \gamma + X$. In general, the magnitude of this uncertainty is much larger than the sum of all the higher twist contributions, so it is very difficult to extract the higher twist contributions.

The Mandelstam invariant variables for subprocesses $q_1 + \bar{q}_2 \rightarrow \pi^+ (\pi^-) + \gamma$ are defined as

$$\hat{s} = (p_1 + p_2)^2, \quad \hat{t} = (p_1 - p_\pi)^2, \quad \hat{u} = (p_1 - p_\gamma)^2. \quad (2.3)$$

In our calculation, we have also neglected the quark masses. We have aimed to calculate the pion production cross section and to fix the differences due to the use of various pion model functions. We have used four different wave functions: the asymptotic wave

function ASY, the Chernyak-Zhitnitsky [23,30], and the wave function in which two non-trivial Gegenbauer coefficients a_2 and a_4 have been extracted from the CLEO data on the $\gamma\gamma^* \rightarrow \pi^0$ transition form factor [31] and Braun-Filyanov pion wave functions[32]. In ref.[31], the authors have used the QCD light-cone sum rules approach and have included into their analysis the NLO perturbative and twist-four corrections. They found that in the model with two nonasymptotic terms, at the scale $\mu_0 = 2.4\text{GeV}$, $a_2 = 0.19, a_4 = -0.14$.

$$\begin{aligned}\Phi_{asy}(x) &= \sqrt{3}f_\pi x(1-x), \quad \Phi_{CZ}(x, \mu_0^2) = 5\Phi_{asy}(2x-1)^2, \\ \Phi_{CLEO}(x, \mu_0^2) &= \Phi_{asy}(x)[1 + 0.19C_2^{3/2}(2x-1) - 0.14C_4^{3/2}(2x-1)], \\ \Phi_{BF}(x, \mu_0^2) &= \Phi_{asy}(x)[1 + 0.66(5(2x-1)^2 - 1) + 0.4687((2x-1)^4 - 14(2x-1)^2 + 1)],\end{aligned}\quad (2.4)$$

where $f_\pi = 0.0923\text{GeV}$ is the pion decay constant. Here, we have denoted by $x \equiv x_1$, the longitudinal fractional momentum carried by the quark within the meson. Then, $x_2 = 1 - x$ and $x_1 - x_2 = 2x - 1$. The pion wave function is symmetric under the replacement $x_1 - x_2 \leftrightarrow x_2 - x_1$. The model functions can be written as

$$\begin{aligned}\Phi_{asy}(x) &= \sqrt{3}f_\pi x(1-x), \\ \Phi_{CZ}(x, \mu_0^2) &= \Phi_{asy}(x) \left[C_0^{3/2}(2x-1) + \frac{2}{3}C_2^{3/2}(2x-1) \right], \\ \Phi_{CLEO}(x, \mu_0^2) &= \Phi_{asy}(x) \left[C_0^{3/2}(2x-1) + 0.19C_2^{3/2}(2x-1) - 0.14C_4^{3/2}(2x-1) \right], \\ \Phi_{BF}(x, \mu_0^2) &= \Phi_{asy}(x) \left[C_0^{3/2}(2x-1) + 0.44C_2^{3/2}(2x-1) + 0.25C_4^{3/2}(2x-1) \right], \\ C_0^{3/2}(2x-1) &= 1, \quad C_2^{3/2}(2x-1) = \frac{3}{2}(5(2x-1)^2 - 1), \\ C_4^{3/2}(2x-1) &= \frac{15}{8}(21(2x-1)^4 - 14(2x-1)^2 + 1).\end{aligned}\quad (2.5)$$

It may be seen that the pion wave function extracted from the experimental data depends on the methods used and their accuracy. Although one may claim that the meson wave function is a process-independent quantity, describing the internal structure of the meson itself, the exploration of different exclusive processes with the same meson leads to a variety of wave functions. This means that the methods employed have shortcomings or do not encompass all the mechanisms important for a given process. Such a situation is pronounced in the case of the pion. It is known that the pion wave function (distribution amplitude-DA) can be expanded over the eigenfunctions of the one-loop Brodsky-Lepage equation, *i.e.*, in terms of the Gegenbauer polynomials $\{C_n^{3/2}(2x-1)\}$,

$$\Phi_\pi(x, Q^2) = \Phi_{asy}(x) \left[1 + \sum_{n=2,4..}^{\infty} a_n(Q^2) C_n^{3/2} (2x-1) \right], \quad (2.6)$$

The evolution of the wave function (DA) on the factorization scale Q^2 is governed by the functions $a_n(Q^2)$,

$$a_n(Q^2) = a_n(\mu_0^2) \left[\frac{\alpha_s(Q^2)}{\alpha_s(\mu_0^2)} \right]^{\gamma_n/\beta_0}, \quad (2.7)$$

$$\frac{\gamma_2}{\beta_0} = \frac{50}{81}, \quad \frac{\gamma_4}{\beta_0} = \frac{364}{405}, \quad n_f = 3.$$

In Eq.(2.7), $\{\gamma_n\}$ are anomalous dimensions defined by the expression,

$$\gamma_n = C_F \left[1 - \frac{2}{(n+1)(n+2)} + 4 \sum_{j=2}^{n+1} \frac{1}{j} \right]. \quad (2.8)$$

The constants $a_n(\mu_0^2) = a_n^0$ are input parameters that form the shape of the wave functions and which can be extracted from experimental data or obtained from the nonperturbative QCD computations at the normalization point μ_0^2 . The QCD coupling constant $\alpha_s(Q^2)$ at the two-loop approximation is given by the expression

$$\alpha_s(Q^2) = \frac{4\pi}{\beta_0 \ln(Q^2/\Lambda^2)} \left[1 - \frac{2\beta_1 \ln \ln(Q^2/\Lambda^2)}{\beta_0^2 \ln(Q^2/\Lambda^2)} \right]. \quad (2.9)$$

Here, Λ is the QCD scale parameter, β_0 and β_1 are the QCD beta function one- and two-loop coefficients, respectively,

$$\beta_0 = 11 - \frac{2}{3}n_f, \quad \beta_1 = 51 - \frac{19}{3}n_f.$$

The cross section for the higher twist subprocess $q_1 \bar{q}_2 \rightarrow \pi^+(\pi^-)\gamma$ is given by the expression

$$\frac{d\sigma}{d\hat{t}}(\hat{s}, \hat{t}, \hat{u}) = \frac{8\pi^2 \alpha_E C_F}{27} \frac{[D(\hat{t}, \hat{u})]^2}{\hat{s}^3} \left[\frac{1}{\hat{u}^2} + \frac{1}{\hat{t}^2} \right], \quad (2.10)$$

where

$$D(\hat{t}, \hat{u}) = e_1 \hat{t} \int_0^1 dx_1 \left[\frac{\alpha_s(Q_1^2) \Phi_\pi(x_1, Q_1^2)}{1-x_1} \right] + e_2 \hat{u} \int_0^1 dx_1 \left[\frac{\alpha_s(Q_2^2) \Phi_\pi(x_1, Q_2^2)}{1-x_1} \right]. \quad (2.11)$$

Here $Q_1^2 = (x_1 - 1)\hat{u}$, and $Q_2^2 = -x_1\hat{t}$, represent the momentum squared carried by the hard gluon in Fig.1, $e_1(e_2)$ is the charge of $q_1(\bar{q}_2)$ and $C_F = \frac{4}{3}$. The higher twist contribution to the large- p_T pion production cross section in the process $pp \rightarrow \pi^+(\pi^-) + \gamma$ is [33]

$$\Sigma_M^{HT} \equiv E \frac{d\sigma}{d^3p} = \int_0^1 \int_0^1 dx_1 dx_2 G_{q_1/h_1}(x_1) G_{q_2/h_2}(x_2) \frac{\hat{s}}{\pi} \frac{d\sigma}{d\hat{t}}(q\bar{q} \rightarrow \pi\gamma) \delta(\hat{s} + \hat{t} + \hat{u}). \quad (2.12)$$

$$\begin{aligned}
\pi E \frac{d\sigma}{d^3p} &= \frac{d\sigma}{dy dp_T^2}, \\
\hat{s} &= x_1 x_2 s, \\
\hat{t} &= x_1 t, \\
\hat{u} &= x_2 u,
\end{aligned} \tag{2.13}$$

$$\begin{aligned}
t &= -m_T \sqrt{s} e^{-y} = -p_T \sqrt{s} e^{-y}, \\
u &= -m_T \sqrt{s} e^y = -p_T \sqrt{s} e^y, \\
x_1 &= -\frac{x_2 u}{x_2 s + t} = \frac{x_2 p_T \sqrt{s} e^y}{x_2 s - p_T \sqrt{s} e^{-y}}, \\
x_2 &= -\frac{x_1 t}{x_1 s + u} = \frac{x_1 p_T \sqrt{s} e^{-y}}{x_1 s - p_T \sqrt{s} e^y},
\end{aligned}$$

where m_T – is the transverse mass of pion, which is given by

$$m_T^2 = m^2 + p_T^2.$$

For a full discussion, we consider a difference Δ^{HT} between the higher twist cross section combinations $\Sigma_{\pi^+}^{HT}$ and $\Sigma_{\pi^-}^{HT}$

$$\Delta_\pi^{HT} = \Sigma_{\pi^+}^{HT} - \Sigma_{\pi^-}^{HT} = E_{\pi^+} \frac{d\sigma}{d^3p}(pp \rightarrow \pi^+ \gamma) - E_{\pi^-} \frac{d\sigma}{d^3p}(pp \rightarrow \pi^- \gamma). \tag{2.14}$$

We have extracted the following higher twist subprocesses contributing to the two covariant cross sections in Eq.(2.12)

$$\frac{d\sigma^1}{d\hat{t}}(u\bar{d} \rightarrow \pi^+ \gamma), \quad \frac{d\sigma^2}{d\hat{t}}(\bar{d}u \rightarrow \pi^+ \gamma), \quad \frac{d\sigma^3}{d\hat{t}}(\bar{u}d \rightarrow \pi^- \gamma), \quad \frac{d\sigma^4}{d\hat{t}}(d\bar{u} \rightarrow \pi^- \gamma), \tag{2.15}$$

By charge conjugation invariance, we have

$$\frac{d\sigma^1}{d\hat{t}}(u\bar{d} \rightarrow \pi^+ \gamma) = \frac{d\sigma^3}{d\hat{t}}(\bar{u}d \rightarrow \pi^- \gamma), \text{ and } \frac{d\sigma^2}{d\hat{t}}(\bar{d}u \rightarrow \pi^+ \gamma) = \frac{d\sigma^4}{d\hat{t}}(d\bar{u} \rightarrow \pi^- \gamma). \tag{2.16}$$

III. THE RUNNING COUPLING APPROACH AND HIGHER TWIST MECHANISM

In this section we shall calculate the integral (2.11) using the running coupling constant method and also discuss the problem of normalization of the higher twist process cross section in the context of the same approach.

As is seen from (2.11), in general, one has to take into account not only the dependence of $\alpha(\hat{Q}_{1,2}^2)$ on the scale $\hat{Q}_{1,2}^2$, but also an evolution of $\Phi(x, \hat{Q}_{1,2}^2)$ with $\hat{Q}_{1,2}^2$. The meson wave function evolves in accordance with a Bethe-Salpeter type equation. Therefore, it is worth noting that, the renormalization scale (argument of α_s) should be chosen equal to $Q_1^2 = (x_1 - 1)\hat{u}$, $Q_2^2 = -x_1\hat{t}$, whereas that factorization scale (Q^2 in $\Phi_M(x, Q^2)$) is taken independent from x , we take $Q^2 = p_T^2$. Such approximation does not change considerably numerical results, but phenomenon considering in this article (effect of infrared renormalons) becomes transparent. The main problem in our investigation is the calculation of integral in (2.11) by the running coupling constant method. The integral in Eq.(2.11) in the framework of the running coupling approach takes the form

$$I(\hat{Q}^2) = \int_0^1 \frac{\alpha_s(\lambda Q^2) \Phi_M(x, Q^2) dx}{1-x}. \quad (3.1)$$

The $\alpha_s(\lambda Q^2)$ has the infrared singularity at $x \rightarrow 1$, if $\lambda = 1 - x$ and as a result integral (3.1) diverges (the pole associated with the denominator of the integrand is fictitious, because $\Phi_M \sim (1 - x)$, and therefore, the singularity of the integrand at $x = 1$ is caused only by $\alpha_s((1 - x)Q^2)$). For the regularization of the integral we express the running coupling at scaling variable $\alpha_s(\lambda Q^2)$ with the aid of the renormalization group equation in terms of the fixed one $\alpha_s(Q^2)$. The renormalization group equation for the running coupling $\alpha \equiv \alpha_s/\pi$ has the form [28]

$$\frac{\partial \alpha(\lambda Q^2)}{\partial \ln \lambda} = -b_2 [\alpha(\lambda Q^2)]^2 - b_3 [\alpha(\lambda Q^2)]^3 \quad (3.2)$$

where

$$b_2 = \frac{1}{12}(33 - 2n_f), \quad b_3 = \frac{1}{48}(306 - 38n_f).$$

The solution of Eq.(3.2) with initial condition

$$\alpha(\lambda)|_{\lambda=1} = \alpha \equiv \alpha_s(Q^2)/\pi$$

is [28]

$$\frac{\alpha(\lambda)}{\alpha} = \left[1 + \alpha b_2 \ln \lambda - \frac{\alpha b_3}{b_2} \left(\frac{\ln \alpha(\lambda)}{\alpha} - \ln \frac{b_2/b_3 + \alpha(\lambda)}{b_2/b_3 + \alpha} \right) \right]^{-1} \quad (3.3)$$

This transcendental equation can be solved iteratively by keeping the leading $\alpha^k \ln^k \lambda$ and next-to-leading $\alpha^k \ln^{k-1} \lambda$ powers. For $\lambda = (1 - x)$ these terms are given by

$$\alpha((1 - x)Q^2) = \frac{\alpha(Q^2)}{1 + \alpha(Q^2)b_2 \ln(1 - x)} - \frac{\alpha^2(Q^2)b_3 \ln[1 + \alpha(Q^2)b_2 \ln(1 - x)]}{b_2[1 + \alpha(Q^2)b_2 \ln(1 - x)]^2} \quad (3.4)$$

The first term in Eq.(3.4) is the solution of the renormalization group Eq.(3.2) with leading power accuracy, whereas the whole expression (3.4) is the solution of Eq.(3.2) with next-to-leading power accuracy. In this work we use only the first term of Eq.(3.4). After substituting Eq.(3.4) into Eq.(2.11) we get

$$\begin{aligned} D(Q^2) &= e_1 \hat{t} \int_0^1 dx_1 \frac{\alpha_s(\lambda Q^2) \Phi_M(x, Q^2)}{1 - x} + e_2 \hat{u} \int_0^1 dx_1 \frac{\alpha_s(\lambda Q^2) \Phi_M(x, Q^2)}{1 - x} = \\ &e_1 \hat{t} \alpha_s(Q^2) \int_0^1 dx_1 \frac{\Phi_M(x, Q^2)}{(1 - x)(1 + \ln \lambda/t)} + e_2 \hat{u} \alpha_s(Q^2) \int_0^1 dx \frac{\Phi_M(x, Q^2)}{(1 - x)(1 + \ln \lambda/t)} = \\ &e_1 \hat{t} \alpha_s(Q^2) \int_0^1 dx \frac{\Phi_{asy}(x) \left[1 + \sum_{2,4,\dots}^\infty a_n(\mu_0^2) \left[\frac{\alpha_s(Q^2)}{\alpha_s(\mu_0^2)} \right]^{\gamma_n/\beta_0} C_n^{3/2} (2x - 1) \right]}{(1 - x)(1 + \ln \lambda/t)} + \\ &e_1 \hat{u} \alpha_s(Q^2) \int_0^1 dx \frac{\Phi_{asy}(x) \left[1 + \sum_{2,4,\dots}^\infty a_n(\mu_0^2) \left[\frac{\alpha_s(Q^2)}{\alpha_s(\mu_0^2)} \right]^{\gamma_n/\beta_0} C_n^{3/2} (2x - 1) \right]}{(1 - x)(1 + \ln \lambda/t)} \end{aligned} \quad (3.5)$$

where $t = 4\pi/\alpha_s(Q^2)\beta_0$

The integral (3.5) is, of course, still divergent, but now it is recasted into a form, which is suitable for calculation. Using the running coupling constant method, it may be found as a perturbative series in $\alpha_s(Q^2)$

$$D(Q^2) \sim \sum_{n=1}^{\infty} \left(\frac{\alpha_s(Q^2)}{4\pi} \right)^n S_n, \quad S_n = C_n \beta_0^{n-1} \quad (3.6)$$

The coefficients C_n of this series demonstrate factorial growth $C_n \sim (n - 1)!$, which might indicate an infrared renormalon nature of divergences in the integral (3.5) and corresponding series (3.6). The procedure for dealing with such ill-defined series is well known; one has to perform the Borel transform of the series [15]

$$B[D](u) = \sum_{n=0}^{\infty} \frac{D_n}{n} u^n,$$

then invert $B[D](u)$ to obtain the resummed expression (the Borel sum) $D(Q^2)$. After the we find directly the resummed expression for $D(Q^2)$. The change of the variable x to

$z = \ln(1 - x)$, as $\ln(1 - x) = \ln\lambda$. Then,

$$D(Q^2) = e_1 \hat{t} \alpha_s(Q^2) t \int_0^1 \frac{\Phi_M(x, Q^2) dx}{(1-x)(t+z)} + e_2 \hat{u} \alpha_s(Q^2) t \int_0^1 \frac{\Phi_M(x, Q^2) dx}{(1-x)(t+z)} \quad (3.7)$$

After the inverse Laplace transformation from $1/(t+z)$ the formula (3.7) becomes simpler

$$\frac{1}{t+z} = \int_0^1 e^{-(t+z)u} du \quad (3.8)$$

then, we obtain

$$D(Q^2) = e_1 \hat{t} \alpha_s(Q^2) t \int_0^1 \int_0^\infty \frac{\Phi_M(x, Q^2) e^{-(t+z)u} du dx}{(1-x)} + \\ e_2 \hat{u} \alpha_s(Q^2) t \int_0^1 \int_0^\infty \frac{\Phi_M(x, Q^2) e^{-(t+z)u} du dx}{(1-x)} \quad (3.9)$$

In the case $\Phi_{asy}(x)$ for $D(\hat{t}, \hat{u})$ we get

$$D(Q^2) = \left(\frac{4\sqrt{3}\pi f_\pi e_1 \hat{t}}{\beta_0} + \frac{4\sqrt{3}\pi f_\pi e_2 \hat{u}}{\beta_0} \right) \left[\int_0^\infty du e^{-tu} \left[\frac{1}{1-u} - \frac{1}{2-u} \right] \right] \quad (3.10)$$

In the case $\Phi_{CZ}(x, Q^2)$ wave function we find

$$D(Q^2) = \left(\frac{4\sqrt{3}\pi f_\pi e_1 \hat{t}}{\beta_0} + \frac{4\sqrt{3}\pi f_\pi e_2 \hat{u}}{\beta_0} \right) \left[\int_0^\infty du e^{-tu} \left[\frac{1}{1-u} - \frac{1}{2-u} + \right. \right. \\ \left. \left. 0.84 \left[\frac{\alpha_s(Q^2)}{\alpha_s(\mu_0^2)} \right]^{50/81} \left[\frac{4}{1-u} - \frac{24}{2-u} + \frac{40}{3-u} - \frac{20}{4-u} \right] \right] \right] \quad (3.11)$$

also in the case $\Phi_{CLEO}(x, Q^2)$ wave function we get

$$D(Q^2) = \left(\frac{4\sqrt{3}\pi f_\pi e_1 \hat{t}}{\beta_0} + \frac{4\sqrt{3}\pi f_\pi e_2 \hat{u}}{\beta_0} \right) \int_0^\infty du e^{-tu} \left[\frac{1}{1-u} - \frac{1}{2-u} + 0.405 \left[\frac{\alpha_s(Q^2)}{\alpha_s(\mu_0^2)} \right]^{50/81} \right. \\ \left. \left[\frac{4}{1-u} - \frac{24}{2-u} + \frac{40}{3-u} - \frac{20}{4-u} \right] - 0.4125 \left[\frac{\alpha_s(Q^2)}{\alpha_s(\mu_0^2)} \right]^{364/405} \right. \\ \left. \left[\frac{8}{1-u} - \frac{120}{2-u} + \frac{560}{3-u} - \frac{1112}{4-u} + \frac{1008}{5-u} - \frac{336}{6-u} \right] \right] \quad (3.12)$$

Eq.(3.1-3.2) is nothing more than Borel sum of the perturbative series (3.6) and the corresponding Borel transform in the case $\Phi_{asy}(x)$ is

$$B[D](u) = \frac{1}{1-u} - \frac{1}{2-u} \quad (3.13)$$

in the case $\Phi_{CZ}(x, Q^2)$ is

$$B[D](u) = \frac{1}{1-u} - \frac{1}{2-u} + 0.84 \left(\frac{\alpha_s(Q^2)}{\alpha_s(\mu_0^2)} \right)^{50/81} \left(\frac{4}{1-u} - \frac{24}{2-u} + \frac{40}{3-u} - \frac{20}{4-u} \right) \quad (3.14)$$

and in the case $\Phi_{CLEO}(x, Q^2)$ is

$$B[D](u) = \frac{1}{1-u} - \frac{1}{2-u} + 0.405 \left(\frac{\alpha_s(Q^2)}{\alpha_s(\mu_0^2)} \right)^{50/81} \left(\frac{4}{1-u} - \frac{24}{2-u} + \frac{40}{3-u} - \frac{20}{4-u} \right) - \\ 0.4125 \left(\frac{\alpha_s(Q^2)}{\alpha_s(\mu_0^2)} \right)^{364/405} \left(\frac{8}{1-u} - \frac{120}{2-u} + \frac{560}{3-u} - \frac{1112}{4-u} + \frac{1008}{5-u} - \frac{336}{6-u} \right) \quad (3.15)$$

The series (3.6) can be recovered by means of the following formula

$$C_n = \left(\frac{d}{du} \right)^{n-1} B[D](u) \big|_{u=0}$$

The Borel transform $B[D](u)$ has poles on the real u axis at $u = 1; 2; 3; 4; 5; 6$, which confirms our conclusion concerning the infrared renormalon nature of divergences in (3.6). To remove them from Eq.(3.11-3.12) some regularization methods have to be applied. In this article we adopt the principal value prescription. We obtain: in the case Φ_{asy}

$$[D(Q^2)]^{res} = \left(\frac{4\sqrt{3}\pi f_\pi e_1 \hat{t}}{\beta_0} + \frac{4\sqrt{3}\pi f_\pi e_2 \hat{u}}{\beta_0} \right) \left[\frac{Li(\lambda)}{\lambda} - \frac{Li(\lambda^2)}{\lambda^2} \right], \quad (3.16)$$

in the case $\Phi_{CZ}(x, Q^2)$

$$[D(Q^2)]^{res} = \left(\frac{4\sqrt{3}\pi f_\pi e_1 \hat{t}}{\beta_0} + \frac{4\sqrt{3}\pi f_\pi e_2 \hat{u}}{\beta_0} \right) \left[\left[\frac{Li(\lambda)}{\lambda} - \frac{Li(\lambda^2)}{\lambda^2} \right] + 0.84 \left(\frac{\alpha_s(Q^2)}{\alpha_s(\mu_0^2)} \right)^{50/81} \right. \\ \left. \left[4 \frac{Li(\lambda)}{\lambda} - 24 \frac{Li(\lambda^2)}{\lambda^2} + 40 \frac{Li(\lambda^3)}{\lambda^3} - 20 \frac{Li(\lambda^4)}{\lambda^4} \right] \right] \quad (3.17)$$

also in the case $\Phi_{CLEO}(x, Q^2)$

$$[D(Q^2)]^{res} = \left(\frac{4\sqrt{3}\pi f_\pi e_1 \hat{t}}{\beta_0} + \frac{4\sqrt{3}\pi f_\pi e_2 \hat{u}}{\beta_0} \right) \left[\left(\frac{Li(\lambda)}{\lambda} - \frac{Li(\lambda^2)}{\lambda^2} \right) + 0.405 \left(\frac{\alpha_s(Q^2)}{\alpha_s(\mu_0^2)} \right)^{50/81} \left(4 \frac{Li(\lambda)}{\lambda} - \right. \right. \\ \left. \left. 24 \frac{Li(\lambda^2)}{\lambda^2} + 40 \frac{Li(\lambda^3)}{\lambda^3} - 20 \frac{Li(\lambda^4)}{\lambda^4} \right) - 0.4125 \left(\frac{\alpha_s(Q^2)}{\alpha_s(\mu_0^2)} \right)^{364/405} \left(8 \frac{Li(\lambda)}{\lambda} - 120 \frac{Li(\lambda^2)}{\lambda^2} + 560 \frac{Li(\lambda^3)}{\lambda^3} - \right. \right. \\ \left. \left. 1112 \frac{Li(\lambda^4)}{\lambda^4} + 1008 \frac{Li(\lambda^5)}{\lambda^5} - 336 \frac{Li(\lambda^6)}{\lambda^6} \right) \right] \quad (3.18)$$

where $Li(\lambda)$ is the logarithmic integral [34], for $\lambda > 1$ defined in its principal value

$$Li(\lambda) = P.V. \int_0^\infty \frac{dx}{\ln x}, \quad \lambda = Q^2/\Lambda^2. \quad (3.19)$$

IV. CONTRIBUTION OF THE LEADING TWIST DIAGRAMS

Regarding the higher twist corrections to the pion production cross section, a comparison of our results with leading twist contributions is crucial. The leading twist subprocesses for the pion production are quark-antiquark annihilation $q\bar{q} \rightarrow g\gamma$, $g \rightarrow \pi^+(\pi^-)$. The corresponding cross section is obtained in

$$\frac{d\sigma}{d\hat{t}}(q\bar{q} \rightarrow gq) = \frac{8}{9}\pi\alpha_E\alpha_s(Q^2)\frac{e_q^2}{\hat{s}^2}\left(\frac{\hat{t}}{\hat{u}} + \frac{\hat{u}}{\hat{t}}\right), \quad (4.1)$$

For the leading-twist contribution, we find

$$\Sigma_M^{LT} \equiv E \frac{d\sigma}{d^3p} = \sum_q \int_0^1 dx_1 dx_2 dz G_{q_1/h_1}(x_1) G_{q_2/h_2}(x_2) D_g^\pi(z) \frac{\hat{s}}{\pi z^2} \frac{d\sigma}{d\hat{t}}(q\bar{q} \rightarrow g\gamma) \delta(\hat{s} + \hat{t} + \hat{u}), \quad (4.2)$$

where

$$\hat{s} = x_1 x_2 s, \quad \hat{t} = \frac{x_1 t}{z}, \quad \hat{u} = \frac{x_2 u}{z}, \quad z = -\frac{x_1 t + x_2 u}{x_1 x_2 s}. \quad (4.3)$$

$D_g^\pi(z) = D_g^{\pi^+}(z) = D_g^{\pi^-}(z)$ represents the gluon fragmentation function into a meson containing a gluon of the same flavor. In the leading twist subprocess, π meson is indirectly emitted from the gluon with the fractional momentum z . The δ function may be expressed in terms of the parton kinematic variables, and the z integration may then be done. The final form for the cross section is

$$\begin{aligned} \Sigma_M^{LT} \equiv E \frac{d\sigma}{d^3p} &= \sum_q \int_{x_{1min}}^1 dx_1 \int_{x_{2min}}^1 dx_2 G_{q_1/h_1}(x_1) G_{q_2/h_2}(x_2) D_g^\pi(z) \times \\ \frac{1}{\pi z} \frac{d\sigma}{d\hat{t}}(q\bar{q} \rightarrow g\gamma) &= \sum_q \int_{x_{1min}}^1 dx_1 \int_{x_{2min}}^1 dx_2 \frac{x_1 G_{q_1/h_1}(x_1) s x_2 G_{q_2/h_2}(x_2)}{-(x_1 t + x_2 u)} \frac{D_g^\pi(z)}{\pi} \frac{d\sigma}{d\hat{t}}(q\bar{q} \rightarrow g\gamma). \end{aligned} \quad (4.4)$$

V. NUMERICAL RESULTS AND DISCUSSION

In this section, the numerical results for higher twist effects which higher twist contributions calculated in the context of the running coupling constant method and of the frozen coupling approximation on the dependence of the chosen meson wave functions in the process $pp \rightarrow \pi^+(or \pi^-)\gamma$ are discussed. In the calculations, the asymptotic Φ_{asy} , Chernyak-Zhitnitsky Φ_{CZ} , the pion wave function, from which two non-trivial Gegenbauer coefficients

a_2 and a_4 have been extracted from the CLEO data on the $\pi^0\gamma$ transition form factor[31] and Braun-Filyanov pion wave function [32] have been used. In the ref.[31], authors have used the QCD light-cone sum rules approach and included into their analysis the NLO perturbative and twist-four corrections. For the higher twist subprocess, we take $q_1 + \bar{q}_2 \rightarrow (q_1\bar{q}_2) + \gamma$ and we have extracted the following four higher twist subprocesses $u\bar{d} \rightarrow \pi^+\gamma$, $\bar{d}u \rightarrow \pi^+\gamma$, $\bar{u}d \rightarrow \pi^-\gamma$, $d\bar{u} \rightarrow \pi^-\gamma$ contributing to $pp \rightarrow \pi^+(or \pi^-)\gamma$ cross sections. For the dominant leading twist subprocess for the pion production, we take the quark-antiquark annihilation $q\bar{q} \rightarrow g\gamma$, in which the π meson is indirectly emitted from the gluon. As an example for the quark distribution function inside the proton, the MRST2003c package [35] has been used. The other problems dealt with are the choice of the QCD scale parameter Λ and the number of the active quark flavors n_f . In our calculations below we shall use the following values of the parameters Λ and μ_0 :

$$\Lambda = 0.25 GeV, \quad \mu_0^2 = 1 GeV^2$$

Also, at the calculations for the Gegenbauer coefficients we use values in the normalization scale $\mu_0^2 = 1 GeV^2$ from [36] The higher twist subprocesses probe the meson wave functions over a large range of Q^2 squared momentum transfer, carried by the gluon. Therefore, in the diagram given in Fig.1 we take $Q_1^2 = (x_1 - 1)\hat{u}$, $Q_2^2 = -x_1\hat{t}$, which we have obtained directly from the higher twist subprocesses diagrams. The same Q^2 has been used as an argument of $\alpha_s(Q^2)$ in the calculation of each diagram. The results of our numerical calculations are plotted in Figs.2-13. First of all, it is very interesting to compare the resummed higher twist cross sections with the ones obtained in the framework of the frozen coupling approximation. In Fig.2, the ratio $R = (\Sigma_{\pi^+}^{HT})^{res}/\Sigma_{\pi^+}^{LT}$ is plotted at $y = 0$ as a function of the pion transverse momentum p_T for the different pion wave functions. First of all, it is seen that the values of R for fixed y and \sqrt{s} depend on the choice of the pion wave function. As seen from Fig.2, the ratio in the region $2 GeV/c < p_T < 24 GeV/c$ is decreasing with an increase in the transverse momentum of the pion, after in the region $24 GeV/c < p_T < 30 GeV/c$ the ratio is increasing with an increase in the transverse momentum of the pion. Fig.3 shows the dependence of the ratio $R = (\Sigma_{\pi^+}^{HT})^{res}/(\Sigma_{\pi^+}^{HT})^0$ as a function of the pion transverse momentum p_T for four different meson wave functions. Here $(\Sigma_{\pi^+}^{HT})^{res}$ is the higher twist cross section calculated in the context of the running coupling method and $(\Sigma_{\pi^+}^{HT})^0$ is the higher twist cross section calculated in the context of the frozen coupling approximation. As shown in Fig.3, the ratio in the region $2 GeV/c < p_T < 30 GeV/c$ is decreasing with an

increase in the transverse momentum of the pion. As is seen from Fig.3, in all wave functions of the mesons, the dependencies of the ratio R on the transverse momentum p_T of the pion demonstrate the same behavior. On the other hand, the higher twist corrections and ratio are very sensitive to the choice of the pion wave function. Also, the distinction between $R(\Phi_{asy}(x))$ with $R(\Phi_{CLEO}(x, Q^2))$, $R(\Phi_{CZ}(x, Q^2))$, $R(\Phi_{BF}(x, Q^2))$ have been calculated. For example, in the case of $\sqrt{s} = 63 \text{ GeV}$, $y = 0$, the distinction between $R(\Phi_{asy}(x))$ with $R(\Phi_i(x, Q^2))$ ($i=CLEO, CZ, BF$) is shown in Table I. Thus, the distinction between $R(\Phi_{asy}(x))$ and $R(\Phi_i(x, Q^2))$ ($i = CLEO, CZ, BF$) is maximum at $p_T = 20 \text{ GeV}/c$, but the distinction between $R(\Phi_{asy}(x))$ with $R(\Phi_i(x, Q^2))$ ($i = CLEO, CZ, BF$) is minimum at $p_T = 2 \text{ GeV}/c$ and increase with an increase in p_T . Such a behavior of R may be explained by reducing all moments of the pion model wave functions to those of $\Phi_{asy}(x)$ for high Q^2 . In Figs.4-5, we have depicted $R = (\Sigma_{\pi^+}^{HT})^{res}/\Sigma_{\pi^+}^{LT}$ and $R=(\Sigma_{\pi^+}^{HT})^{res}/(\Sigma_{\pi^+}^{HT})^0$ as a function of the rapidity y of the pion at $\sqrt{s} = 63 \text{ GeV}$ and $p_T = 5 \text{ GeV}/c$. At $\sqrt{s} = 63 \text{ GeV}$ and $p_T = 5 \text{ GeV}/c$, the pion rapidity lies in the region $-2.52 \leq y \leq 2.52$. As is seen from Fig.4 the ratio for all wave functions increase with an increase of the y rapidity of the pion. But, as is seen from Fig.5, in the region $(-2.52 \leq y \leq -1.92)$, the ratio for all wave functions increase and it has a maximum approximately at the point $y = -1.92$. Besides that, the ratio is decrease with an increase in the y rapidity of the pion. As is seen from Figs.4-5, the ratios R are very sensitive to the choice of the meson wave functions. In Fig.6, we show the ratio $r=(\Delta_{\pi}^{HT})^{res}/(\Delta_{\pi}^{HT})^0$, where $\Delta_{\pi}^{HT} = \Sigma_{\pi^+}^{HT} - \Sigma_{\pi^-}^{HT}$, as a function of the pion transverse momentum p_T for four different pion wave functions. As is seen from Fig.6, when the transverse momentum of the pion is increasing, the ratio r is decreasing. We have obtained very interesting results. The calculations show that the ratio $R(\Phi_i(x, Q^2))/R(\Phi_{asy}(x))$, ($i=CLEO, CZ, BF$) for all the transverse momentum p_T of the pion identical equivalent to ratio $r(\Phi_i(x, Q^2)/r(\Phi_{asy}(x))$, ($i=CLEO, CZ, BF$). In Fig.7, we show the ratio $r=(\Delta_{\pi}^{HT})^{res}/(\Delta_{\pi}^{HT})^0$, where $\Delta_{\pi}^{HT} = \Sigma_{\pi^+}^{HT} - \Sigma_{\pi^-}^{HT}$ as a function of the rapidity y of the pion at $\sqrt{s} = 63 \text{ GeV}$ and $p_T = 5 \text{ GeV}/c$. As is seen from Fig.7, the ratio r are very sensitive to the choice of meson wave functions. We have also carried out comparative calculations in the center-of-mass energy $\sqrt{s} = 630 \text{ GeV}$. In Fig.8, the ratio $R = (\Sigma_{\pi^+}^{HT})^{res}/\Sigma_{\pi^+}^{LT}$ is plotted at $y = 0$ as a function of the pion transverse momentum p_T for the different pion wave functions. First of all, it is seen that the values of R for fixed y and \sqrt{s} depend on the choice of the pion wave function. Fig.9 shows the dependence of the ratio $R = (\Sigma_{\pi^+}^{HT})^{res}/(\Sigma_{\pi^+}^{HT})^0$ as

a function of the pion transverse momentum p_T for four different meson wave functions. As is shown in Fig.9, the ratio in the region of $20 \text{ GeV}/c < p_T < 300 \text{ GeV}/c$ is decreasing with an increase in the transverse momentum of the pion. As is seen from Fig.9, for all wave functions of the mesons, the dependencies of the ratio R on the transverse momentum p_T of the pion demonstrate the same behavior. On the other hand, the higher twist corrections and ratio are very sensitive to the choice of the pion wave function. Also, the distinction between $R(\Phi_{asy}(x))$ with $R(\Phi_{CLEO}(x, Q^2))$, $R(\Phi_{CZ}(x, Q^2))$, $R(\Phi_{BF}(x, Q^2))$ have been calculated. For example, in the case of $\sqrt{s} = 630 \text{ GeV}$, $y = 0$, the distinction between $R(\Phi_{asy}(x))$ with $R(\Phi_i(x, Q^2))$ (i=CLEO, CZ, BF) is shown in Table III. Thus, the distinction between $R(\Phi_{asy}(x))$ with $R(\Phi_i(x, Q^2))$, (i=CZ, CLEO, BF) is maximum at $p_T = 200 \text{ GeV}/c$, but the distinction between $R(\Phi_{asy}(x))$ with $R(\Phi_{CZ}(x, Q^2))$, $R(\Phi_{CLEO}(x, Q^2))$, $R(\Phi_{BF}(x, Q^2))$ is minimum at $p_T = 20 \text{ GeV}/c$ and increase with an increase in p_T . Such a behavior of R may be explained by reducing all moments of the pion model wave functions to those of $\Phi_{asy}(x)$ for high Q^2 . In Figs.10-11, we have depicted $R = (\Sigma_{\pi^+}^{HT})^{res}/\Sigma_{\pi^+}^{LT}$ and $R = (\Sigma_{\pi}^{HT})^{res}/(\Sigma_{\pi}^{HT})^0$ as a function of the rapidity y of the pion at $\sqrt{s} = 630 \text{ GeV}$ and $p_T = 50 \text{ GeV}/c$. At $\sqrt{s} = 630 \text{ GeV}$ and $p_T = 50 \text{ GeV}/c$, the pion rapidity lies in the region $-2.52 \leq y \leq 2.52$. As is seen from Fig.10 the ratio for all wave functions increase with an increase of the y rapidity of the pion. But, as is seen from Fig.11, in the region $(-2.52 \leq y \leq -1.92)$, the ratio for all wave functions increase and it has a maximum approximately at the point $y = -1.92$. After that, the ratio is decrease with an increase of the y rapidity of the pion. As is seen from Figs.10-11, the ratios R are very sensitive to the choice of meson wave functions. In Fig.12, we show the ratio $r = (\Delta_{\pi}^{HT})^{res}/(\Delta_{\pi}^{HT})^0$, where $\Delta_{\pi}^{HT} = \Sigma_{\pi^+}^{HT} - \Sigma_{\pi^-}^{HT}$ as a function of the pion transverse momentum p_T for four different pion wave functions. From Fig.12 we see that when the transverse momentum of the pion is increasing, the ratio r is decreasing. As is seen from Fig.12 the ratio r are sensitive to the choice of the pion wave function. Also, we have calculated the distinction between $R(\Phi_{asy}(x))$ with $R(\Phi_{CLEO}(x, Q^2))$, $R(\Phi_{CZ}(x, Q^2))$, $R(\Phi_{BF}(x, Q^2))$. For example, in the case of $\sqrt{s} = 630 \text{ GeV}$, $p_T = 50$ the distinction between $R(\Phi_{asy}(x))$ with $R(\Phi_i(x, Q^2))$ is presented in Table IV. The calculations show that the ratio $R(\Phi_i(x, Q^2))/R(\Phi_{asy}(x))$, (i=CLEO, CZ, BF) for all values of the transverse momentum p_T of the pion identical equivalent to ratio $r(\Phi_i(x, Q^2))/r(\Phi_{asy}(x))$. In Fig.13, we have depicted $r = (\Delta_{\pi}^{HT})^{res}/(\Delta_{\pi}^{HT})^0$ as a function of the rapidity y of the pion at $\sqrt{s} = 630 \text{ GeV}$ and $p_T = 50 \text{ GeV}/c$. At $\sqrt{s} = 630 \text{ GeV}$ and $p_T = 50 \text{ GeV}/c$, the pion rapidity lies in the region

$-2.52 \leq y \leq 2.52$. As is seen from Fig.13, in the region $(-2.52 \leq y \leq -1.92)$, the ratio for all wave functions increase and it has a maximum approximately at the point $y = -1.92$. After that, the ratio is decrease with an increase in the y rapidity of the pion. As is seen from Fig.13, the ratio r is sensitive to the choice of meson wave functions.

VI. CONCLUDING REMARKS

In this work we have calculated the single meson inclusive production via higher twist mechanism and obtained the expressions for the subprocess $q\bar{q} \rightarrow M\gamma$ cross section for mesons with symmetric wave functions. For calculation of the cross section we have applied the running coupling constant method and revealed infrared renormalon poles in the cross section expression. Infrared renormalon induced divergences have been regularized by means of the principal value prescription and the resummed expression (the Borel sum) for the higher twist cross section has been found. The results of our numerical calculations have been plotted in Figs.2-13. As seen from Figs.2-13 the ratios R and r are very sensitive to the choice of the pion wave function. The resummed higher twist cross section differs from that found using the frozen coupling approximation, in some region, considerably. Also we demonstrated that higher twist contributions to single meson production cross section in the proton-proton collisions have important phenomenological consequences. We have obtained very interesting results. The ratio R for all values of the transverse momentum p_T and of the rapidity of the pion identical equivalent to ratio r . Our investigation enables us to conclude that the higher twist pion production cross section in the proton-proton collisions depends on the form of the pion model wave functions and may be used for their study. Analysis of our calculations shows that cross sections of leading twist is larger than the higher twist cross sections in 2-4 order. In some region of transverse momentum of the pion, the higher twist cross section calculated in the context of the running coupling method is comparable with the cross sections of leading twist. Further investigations are needed in order to clarify the role of high twist effects in QCD. We have demonstrated that the resummed result depends

on the pion model wave functions used in calculations.

VII. REFERENCES

- [1] G.'t. Hooft, in The Whys of Subnuclear Physics, Erice, 1977, edited by A. Zichichi (Plenum, New York, 1979), p.94
- [2] A. H. Muller, Nucl. Phys. **B250**, 327 (1985); Phys. Lett. **B308**, 355 (1993).
- [3] V. I. Zakharov, Nucl. Phys. **B385**, 452 (1992).
- [4] M. Beneke, Phys. Rep. **317**, 1 (1999).
- [5] G. Grunberg, Phys. Lett. **95B**, 70 (1980); **110B**, 501(E), (1982); Phys. Rev. **D29**, 2315 (1984).
- [6] P. M. Stevenson, Phys. Rev. **D23**, 2916 (1981).
- [7] S. J. Brodsky, G. P. Lepage and P. B. Mackenzie, Phys. Rev. **D28**, 228 (1983); G. P. Lepage and P. B. Mackenzie, *ibid.* **48**, 2250 (1993).
- [8] G. Grunberg and A. L. Kataev, Phys. Lett **B279**, 352 (1992).
- [9] S. J. Brodsky and J. Rathsman, hep-ph/9906339.
- [10] H. J. Lu, and C. A. R. Sa de Melo, Phys. Lett **B273**, 260 (1991); **285**, 399(E) (1992); H. J. Lu, Phys. Rev. **D45**, 1217 (1992); Ph. D. thesis, Stanford, 1992, SLAC-0406
- [11] C. P. Lepage and P. B. Mackenzie Phys. Rev. **D48**, 2250 (1993).
- [12] S. J. Brodsky and H. J. Lu, Phys. Rev. **D51**, 3652 (1995).
- [13] J. Rathsman, Phys. Rev. **D54**, 3420 (1996).
- [14] M. Neubert, Phys. Rev. **D51**, 5924 (1995).
- [15] M. Beneke and V. M. Braun, Phys. Lett **B348**, 513 (1995); P. Ball, M. Beneke and V. M. Braun, Nucl. Phys. **B452**, 563 (1995); M. Beneke, Nucl. Phys. **B405**, 563 (1993).
- [16] C. N. Lovett-Turner and C. J. Maxwell, Nucl. Phys. **B432**, 147 (1994).
- [17] S. J. Brodsky, J. Ellis, E. Gardi, M. Karliner, and M. A. Samuel, Phys. Rev. **D56**, 6980 (1997).
- [18] S. J. Brodsky, G. T. Gabadadze, A. L. Kataev, and H. J. Lu, Phys. Lett. **B372**, 133 (1996).
- [19] S. J. Brodsky, M. Melles, and J. Rathsman, Phys. Rev. **D60**, 096006 (1999).
- [20] S. J. Brodsky, M. Melles, and J. Rathsman, Phys. Rev. **D58**, 116006 (1998).
- [21] S. J. Brodsky, R. Blankenbecler and J. F. Gunion, Phys. Rev. **D6**, 2651 (1972); S. J. Brodsky

- and G. R. Farrar, Phys. Rev. Lett. **31**, 1153 (1973).
- [22] G. L. Lepage and S. J. Brodsky, Phys. Rev. **D22**, 2157 (1980).
 - [23] V. L. Chernyak and A. R. Zhitnitsky, Phys. Rep. **112**, 173 (1980).
 - [24] E. L. Berger and S. J. Brodsky, Phys. Rev. Lett. **42**, 940 (1979); E.L. Berger, Z.Phys. **C4**, 289 (1980).
 - [25] V. N. Baier and A. Grozin, Phys. Lett. **B96**, 181 (1980); S. Gupta, Phys. Rev. **D24**, 1169 (1981).
 - [26] S. S. Agaev, Eur.Phys.J.**C1**, 321 (1998).
 - [27] A. I. Ahmadov, I. Boztosun, R. Kh. Muradov, A. Soylu and E. A. Dadashov, Int. J. Mod. Phys. **E15**, 1209 (2006); hep-ph/0607238.
 - [28] H. Contopanagos and G. Sterman, Nucl.Phys. **B419**, 77 (1994).
 - [29] W. Greiner, S. Schramm and E. Stein, Quantum Chromodynamics, Berlin, Germany, Springer 2002, 2 Edition, 551pp.
 - [30] V. L. Chernyak and A. R. Zhitnitsky, Nucl. Phys. **B201**, 492 (1982); V. L. Chernyak, A. R. Zhitnitsky and I. R. Zhitnitsky, Nucl. Phys. **B204**, 477 (1982).
 - [31] A. Schmedding and O. Yakovlev, Phys. Rev. **D62**, 116002 (2000), hep-ph/9905392.
 - [32] V. M. Braun and I. F. Filyanov, Z. Phys, **C44**, 157 (1989).
 - [33] J. F. Owens, Rev. Mod. Phys. **59**, 465 (1987).
 - [34] A. Erdelyi, Higher transcendental functions,v.2, McGraw-Hill Book Company, New York, 1953
 - [35] MRST2003c.f can be obtained from <http://durpdg.dur.ac.uk/hepdata/pdf.html>. See also, A. D. Martin, R. G. Roberts, W. J. Stirling and R. S.Thorne, hep-ph/0307262; R. S.Thorne, hep-ph/0309343.
 - [36] A. P. Bakulev, S. V. Mikhailov and N. G. Stefanis, Phys. Rev. **D73**, 056002 (2006).

$p_T, GeV/c$	$\frac{R(\Phi_{CLEO}(x, Q^2))}{R(\Phi_{asy}(x))}$	$\frac{R(\Phi_{CZ}(x, Q^2))}{R(\Phi_{asy}(x))}$	$\frac{R(\Phi_{BF}(x, Q^2))}{R(\Phi_{asy}(x))}$
2	1.008	0.298	0.63
6	7.854	0.508	2.00
20	23.322	8.03	5.406

TABLE I: The distinction between $R(\Phi_{asy}(x))$ with $R(\Phi_i(x, Q^2))$ (i=CLEO, CZ, BF) at c.m. energy $\sqrt{s} = 63 \text{ GeV}$.

y	$\frac{R(\Phi_{CLEO}(x, Q^2))}{R(\Phi_{asy}(x))}$	$\frac{R(\Phi_{CZ}(x, Q^2))}{R(\Phi_{asy}(x))}$	$\frac{R(\Phi_{BF}(x, Q^2))}{R(\Phi_{asy}(x))}$
-2.52	0.639	11.064	8.693
-1.92	0.345	0.28	0.567
0.78	0.076	0.959	6.462

TABLE II: The distinction between $R(\Phi_{asy}(x))$ with $R(\Phi_i(x, Q^2))$ (i=CLEO, CZ, BF) at c.m. energy $\sqrt{s} = 63 \text{ GeV}$ and $p_T = 5 \text{ GeV}/c$.

$p_T, GeV/c$	$\frac{R(\Phi_{CLEO}(x, Q^2))}{R(\Phi_{asy}(x))}$	$\frac{R(\Phi_{CZ}(x, Q^2))}{R(\Phi_{asy}(x))}$	$\frac{R(\Phi_{BF}(x, Q^2))}{R(\Phi_{asy}(x))}$
20	0.954	0.305	0.627
60	3.374	0.516	1.61
200	7.549	3.809	3.917

TABLE III: The distinction between $R(\Phi_{asy}(x))$ with $R(\Phi_i(x, Q^2))$ (i=CLEO, CZ, BF) at c.m. energy $\sqrt{s} = 630 \text{ GeV}$.

y	$\frac{r(\Phi_{CLEO}(x, Q^2))}{r(\Phi_{asy}(x))}$	$\frac{r(\Phi_{CZ}(x, Q^2))}{r(\Phi_{asy}(x))}$	$\frac{r(\Phi_{BF}(x, Q^2))}{r(\Phi_{asy}(x))}$
-2.52	0.143	4.819	4.096
-1.92	0.786	0.303	0.581
0.78	0.345	0.87	3.713

TABLE IV: The distinction between $R(\Phi_{asy}(x))$ with $R(\Phi_i(x, Q^2))$ (i=CLEO, CZ, BF) at c.m. energy $\sqrt{s} = 630 \text{ GeV}$ and $p_T = 50 \text{ GeV}/c$.

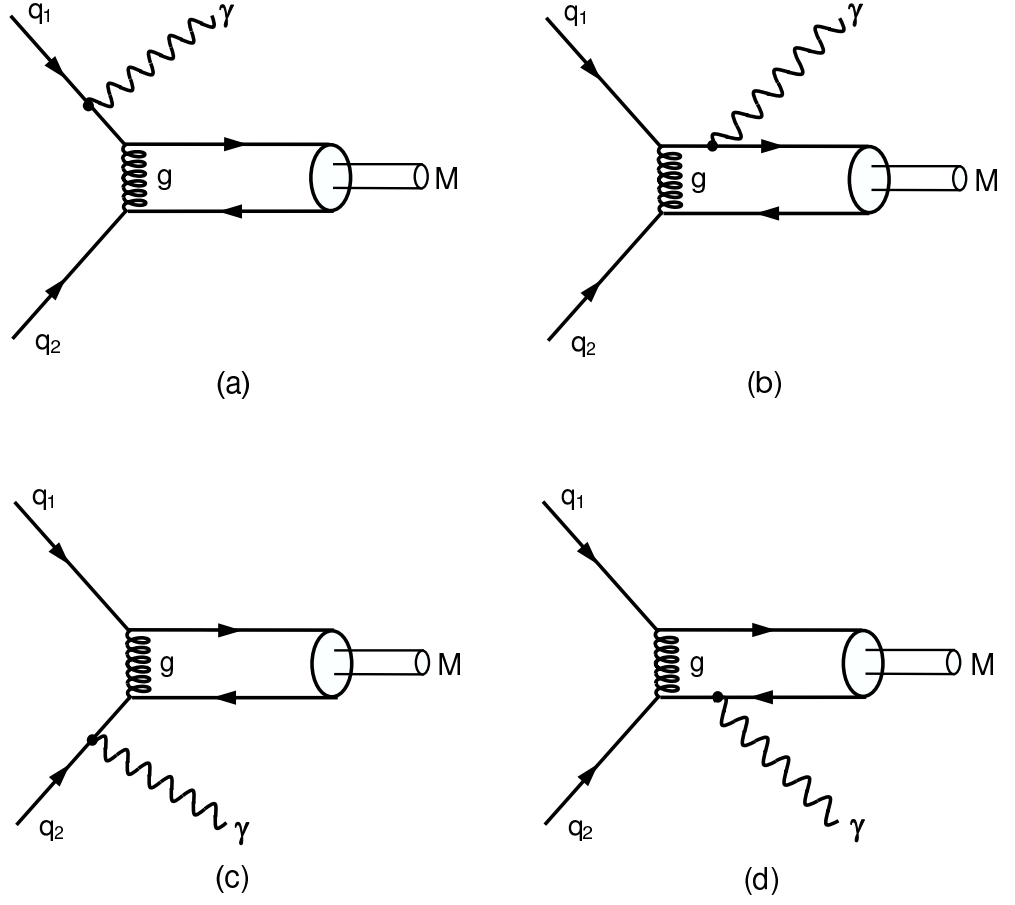


FIG. 1: Feynman diagrams for the higher twist subprocess, $q_1 q_2 \rightarrow \pi^+ (\text{or } \pi^-) \gamma$.

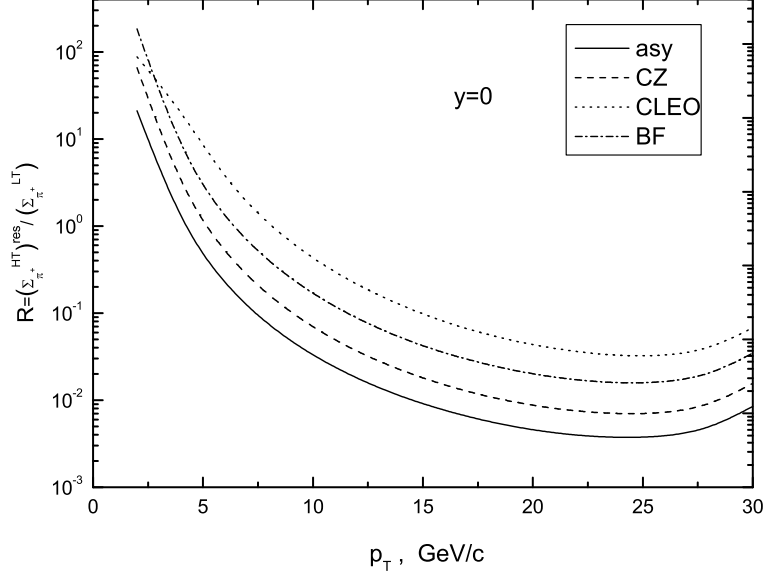


FIG. 2: Ratio $R = (\Sigma_{\pi^+}^{HT})^{res}/(\Sigma_{\pi^+}^{LT})$, where the higher twist contributions are calculated for the pion rapidity $y = 0$ at the c.m. energy $\sqrt{s} = 63 \text{ GeV}$, as a function of the pion transverse momentum, p_T .

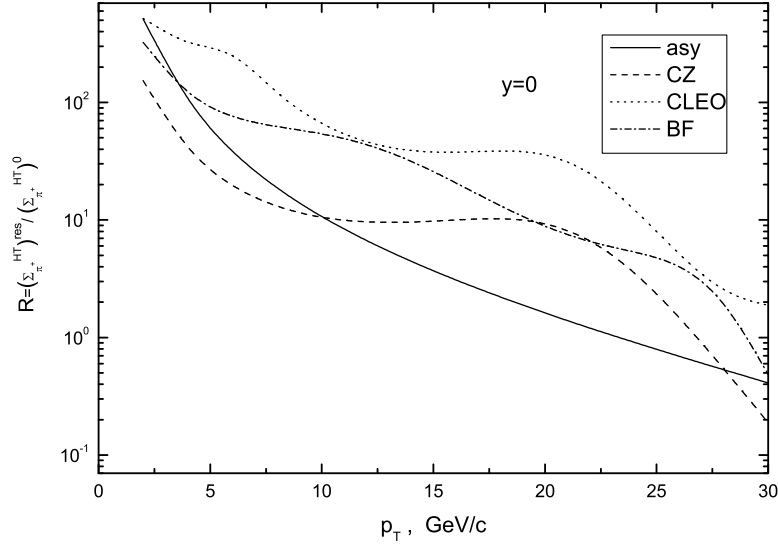


FIG. 3: Ratio $R = (\Sigma_{\pi^+}^{HT})^{res}/(\Sigma_{\pi^+}^{HT})^0$, where higher twist contributions are calculated for the pion rapidity $y = 0$ at the c.m. energy $\sqrt{s} = 63 \text{ GeV}$, as a function of the pion transverse momentum, p_T .

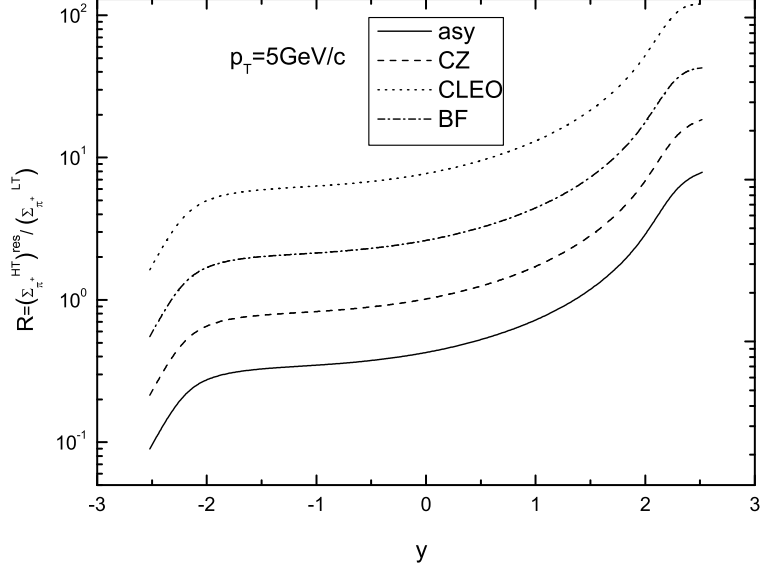


FIG. 4: Ratio $R = (\Sigma_{\pi^+}^{HT})^{res}/(\Sigma_{\pi^+}^{LT})$, as a function of the y rapidity of the pion at the transverse momentum of the pion $p_T = 5 \text{ GeV}/c$, at the c.m. energy $\sqrt{s} = 63 \text{ GeV}$.

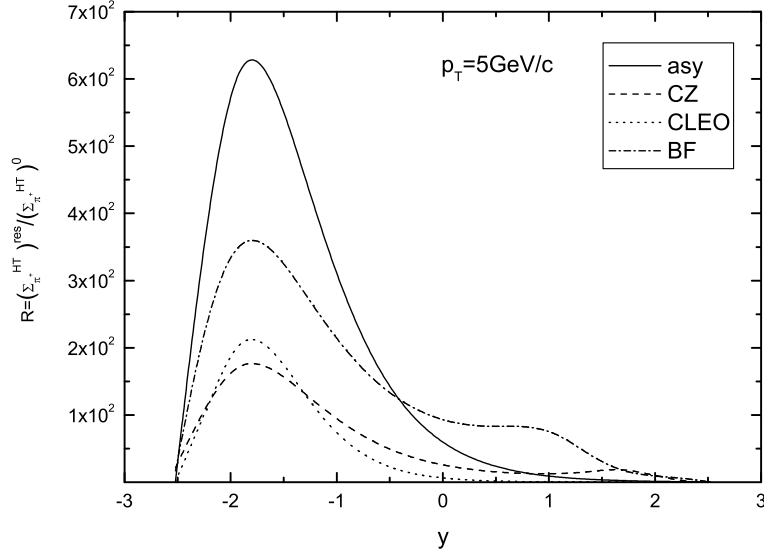


FIG. 5: Ratio $R = (\Sigma_{\pi^+}^{HT})^{res}/(\Sigma_{\pi^+}^{HT})^0$, as a function of the y rapidity of the pion at the transverse momentum of the pion $p_T = 5 \text{ GeV}/c$, at the c.m. energy $\sqrt{s} = 63 \text{ GeV}$.

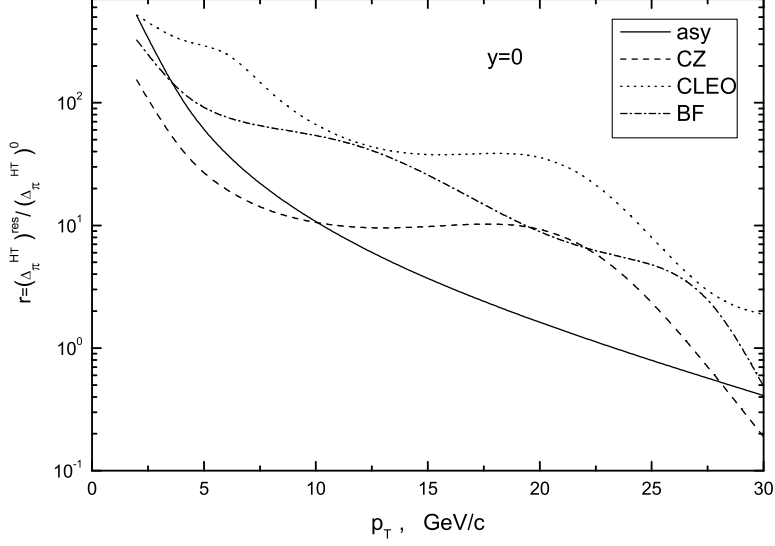


FIG. 6: Ratio $r = (\Delta_\pi^{HT})^{res}/(\Delta_\pi^{HT})^0$, where the higher twist contributions are calculated for the pion rapidity $y = 0$ at the c.m. energy $\sqrt{s} = 63 \text{ GeV}$, as a function of the pion transverse momentum, p_T .

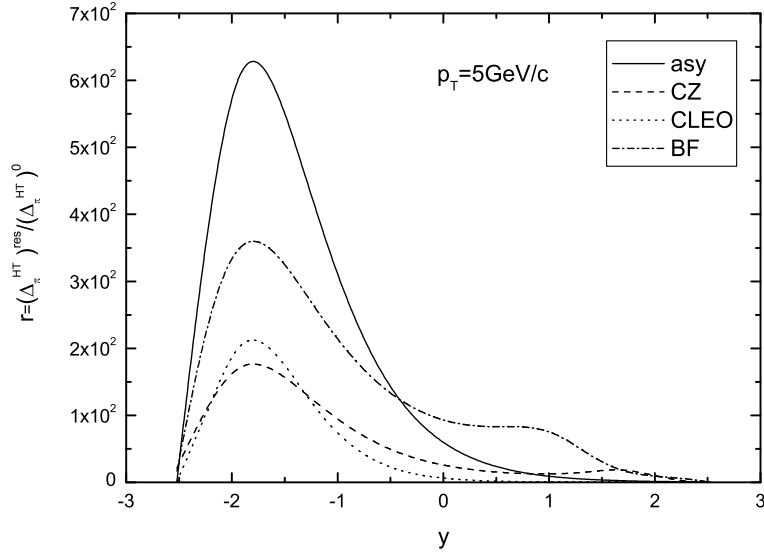


FIG. 7: Ratio $r = (\Delta_\pi^{HT})^{res}/(\Delta_\pi^{HT})^0$, as a function of the y rapidity of the pion at the transverse momentum of the pion $p_T = 5 \text{ GeV}/c$, at the c.m. energy $\sqrt{s} = 63 \text{ GeV}$.

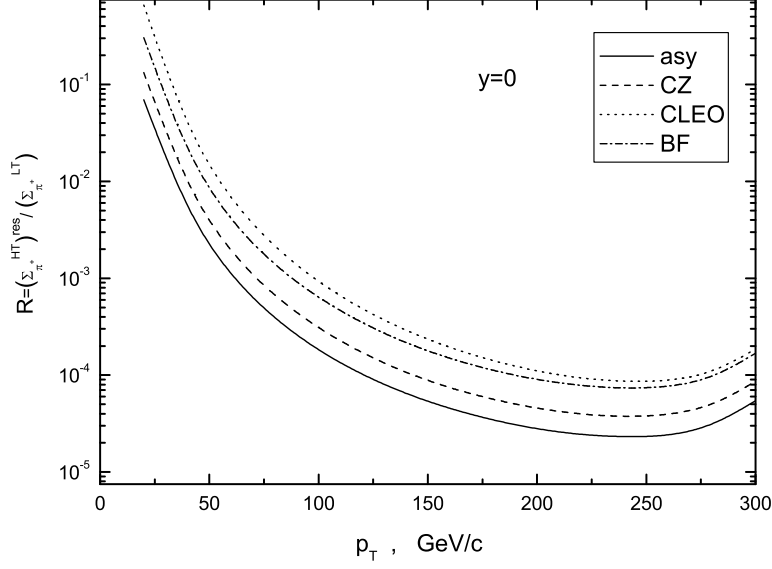


FIG. 8: Ratio $R = (\Sigma_{\pi^+}^{HT})^{res}/(\Sigma_{\pi^+}^{LT})$, where higher twist contributions are calculated for the pion rapidity $y = 0$ at the c.m. energy $\sqrt{s} = 630 \text{ GeV}$, as a function of the pion transverse momentum, p_T .

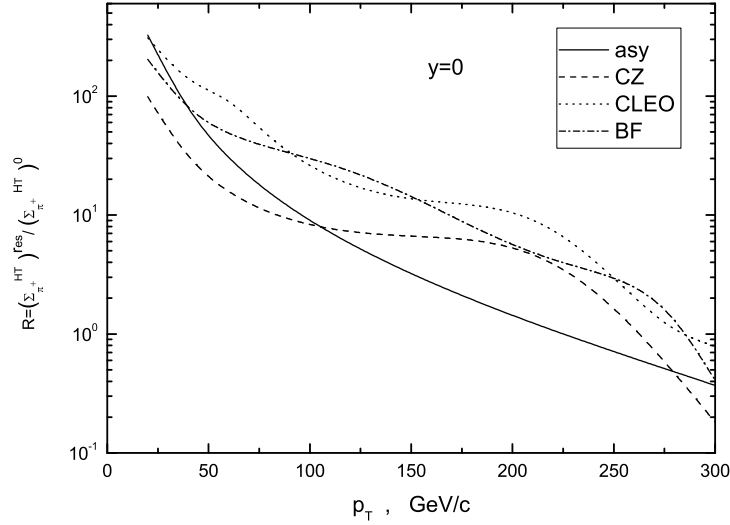


FIG. 9: Ratio $R = (\Sigma_{\pi^+}^{HT})^{res}/(\Sigma_{\pi^+}^{HT})^0$, where higher twist contributions are calculated for the pion rapidity $y = 0$ at the c.m. energy $\sqrt{s} = 63 \text{ GeV}$, as a function of the pion transverse momentum, p_T .

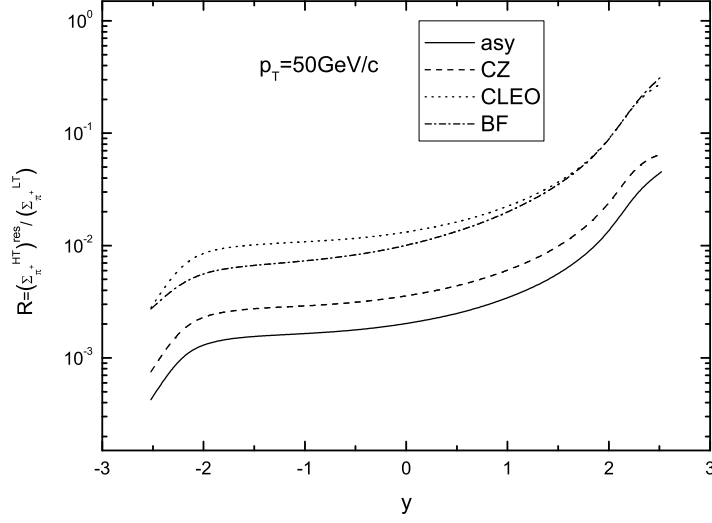


FIG. 10: Ratio $R = (\Sigma_{\pi^+}^{HT})^{res} / (\Sigma_{\pi^+}^{LT})$, as a function of the y rapidity of the pion at the transverse momentum of the pion $p_T = 50 \text{ GeV}/c$, at the c.m. energy $\sqrt{s} = 630 \text{ GeV}$.

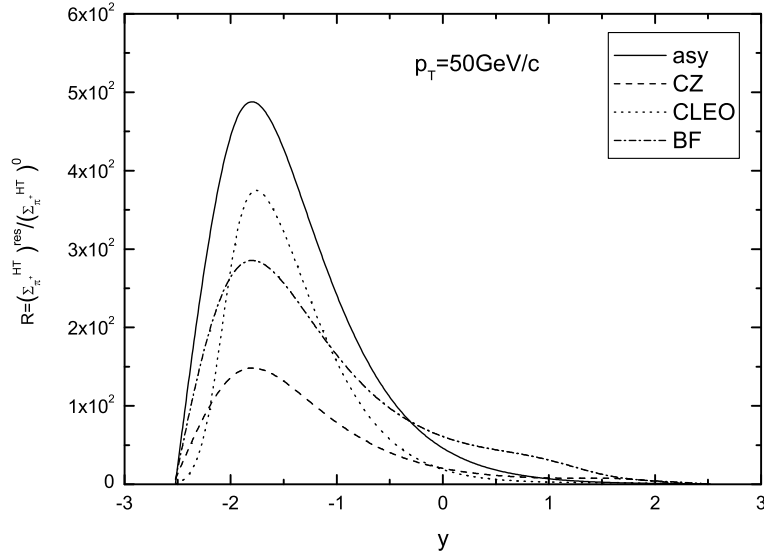


FIG. 11: Ratio $R = (\Sigma_{\pi^+}^{HT})^{res} / (\Sigma_{\pi^+}^{HT})^0$, as a function of the y rapidity of the pion at the transverse momentum of the pion $p_T = 50 \text{ GeV}/c$, at the c.m. energy $\sqrt{s} = 630 \text{ GeV}$.

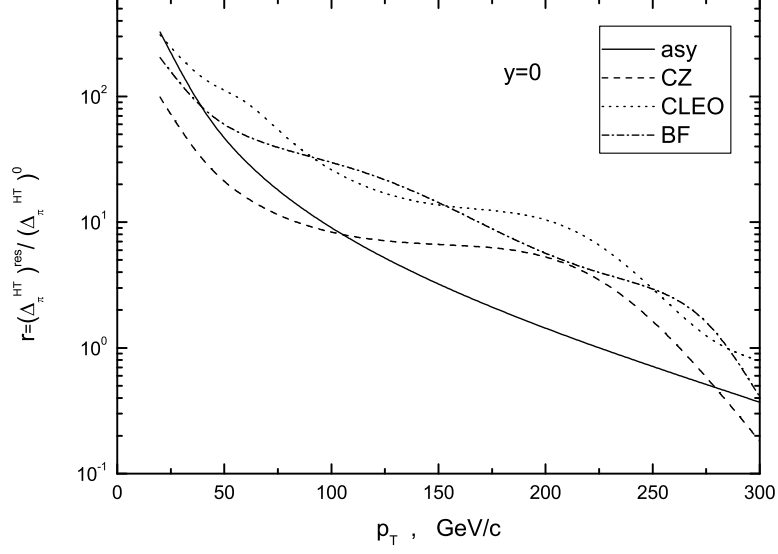


FIG. 12: Ratio $r = (\Delta_\pi^{HT})^{res} / (\Delta_\pi^{HT})^0$, where higher twist contributions are calculated for the pion rapidity $y = 0$ at the c.m. energy $\sqrt{s} = 630 \text{ GeV}$, as a function of the pion transverse momentum, p_T .

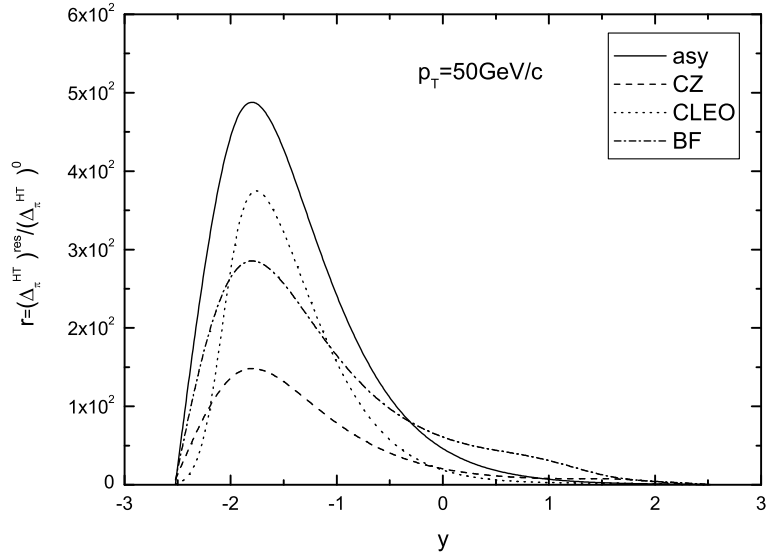


FIG. 13: Ratio $r = (\Delta_\pi^{HT})^{res} / (\Delta_\pi^{HT})^0$, as a function of the y rapidity of the pion at the transverse momentum of the pion $p_T = 50 \text{ GeV}/c$, at the c.m. energy $\sqrt{s} = 630 \text{ GeV}$.